Biomechanics and Modeling in Mechanobiology (2021) 20:2013–2030
https://doi.org/10.1007/s10237-021-01491-z

ORIGINAL PAPER

Loss of longitudinal superiority marks the microarchitecture deterioration of osteoporotic cancellous bones

Zhenzi Li[1] · Pan Liu[1] · Yanan Yuan[1] · Xiaoxiao Liang[2] · Jun Lei[2] · Xiaobin Zhu[2] · Zuoqi Zhang[1,3,4] · Lin Cai[2]

Received: 26 February 2021 / Accepted: 5 July 2021 / Published online: 26 July 2021
© The Author(s), under exclusive licence to Springer-Verlag GmbH Germany, part of Springer Nature 2021

Abstract

Osteoporosis (OP), a skeletal disease making bone mechanically deteriorate and easily fracture, is a global public health issue due to its high prevalence. It has been well recognized that besides bone loss, microarchitecture degradation plays a crucial role in the mechanical deterioration of OP bones, but the specific role of microarchitecture in OP has not been well clarified and quantified from mechanics perspective. Here, we successfully decoupled and identified the specific roles of microarchitecture, bone mass and tissue property in the failure properties of cancellous bones, through μCT-based digital modeling and finite element method simulations on bone samples from healthy and ovariectomy-induced osteoporotic mice. The results show that the microarchitecture of healthy bones exhibits longitudinal superiority in mechanical properties such as the effective stiffness, strength and toughness, which fits them well to bearing loads along their longitudinal direction. OP does not only reduce bone mass but also impair the microarchitecture topology. The former is mainly responsible for the mechanical degradation of bones in magnitude, wherever the latter accounts for the breakdown of their function-favorable anisotropy, the longitudinal superiority. Hence, we identified the microarchitecture-deterioration-induced directional mismatch between material and loading as a hazardous feature of OP and defined a longitudinal superiority index as measurement of the health status of bone microarchitecture. These findings provide useful insights and guidelines for OP diagnosis and treat assessment.

Keywords Trabecular bone · Ternary framework · Bone loss · Structure–function relation · Damage and fracture · Longitudinal superiority index

1 Introduction

Osteoporosis (OP) is a skeletal disease manifesting low bone strength and high risk of bone fracture (Lin and Lane 2004; Rachner et al. 2011). Today OP has become an important public concern all over the world, with more than 200 million people worldwide affected by OP (Lin and Lane 2004). As the global population is fast aging, the number of people suffering from OP has been increasing every year, which brings a huge economic burden to the family and the national medical system (Becker et al. 2010). Cancellous bone, also called trabecular or sponge bone, is a kind of open cell porous material rich and dominant around major joints such as spine, hip and wrist, owning important mechanical functions such as distributing load and absorbing impact energy (Keaveny et al. 2001). Compared with cortical (compact) bone, cancellous bone has a low weight and large surface area per volume, contains many blood vessels and red bone marrow and constructs an active site for metabolic and hematopoiesis activities. Therefore, the responses and

✉ Xiaobin Zhu
xiaobinzhu@whu.edu.cn

✉ Zuoqi Zhang
zhang_zuoqi@whu.edu.cn

1 Department of Mechanical Engineering, School of Civil Engineering, Wuhan University, Wuhan 430072, People's Republic of China

2 Zhongnan Hospital of Wuhan University, Wuhan 430071, People's Republic of China

3 Engineering Research Centre on Building Examination and Reinforcement Technology (Ministry of Education), Wuhan University, Wuhan 430071, People's Republic of China

4 School of Mechanical and Aerospace Engineering, Nanyang Technological University, Singapore 637551, Singapore

activities of osteoblasts and osteoclasts are especially quick and active in cancellous bones, and consequently, they are more sensitive and susceptible to OP (Fonseca et al. 2014; Riggs and Melton 1995). This is why OP-induced bone fractures usually happen in the cancellous bone dominant positions such as hip, spine and wrist (Ciarelli et al. 2000; Hambli et al. 2012; Homminga et al. 2002; Jordan et al. 2003). Hence, in-depth studies on the mechanical deterioration of cancellous bone with OP are essential and crucial for OP prevention, diagnosis and treatment.

Now bone mineral density (BMD) is the most widely utilized measurement for the diagnosis and assessment of OP in clinics. BMD is a good index measuring the overall bone mass, but does not reflect other aspects of bone such as microarchitecture and tissue properties (Licata 2009). Consequently, BMD can only account for approximately 70% of bone strength, and fair and negative correlation between BMD decrease and bone fracture has been reported (Cummings et al. 2002; Delmas and Seeman 2004). To complement BMD, the concept of bone quality was proposed in clinics to better elucidate the bone strength. Bone quality is a general terminology covering many aspects of bone, for instance, microarchitecture, remodeling rate, properties of collagen, and age (Donnelly 2011; Fonseca et al. 2014; McNamara 2010; Seeman and Delmas 2006). Consequently, it is difficult to quantify it with a scalar or tensor variable, and thus, it is almost impossible to establish a closed-form expression within the "bone mass-bone quality" binary framework to quantify the mechanical deterioration of OP bones. Cancellous bone can be considered as a composite consisting of bone tissue and porosity, and the composite theory tells us that a ternary framework "bone mass-microarchitecture-tissue property" (Liu et al. 2019; McNamara 2010; Nyman and Vashishth 2018) is better to investigate the mechanical properties of cancellous bones, as illustrated in Fig. 1. In the ternary framework, the bone mass can be quantitatively characterized by a scalar variable such as bone volume fraction (BV/TV, the bone tissue volume divided by the apparent total volume), or BMD. The microarchitecture can be quantitatively represented by some histomorphometric parameters (e.g., trabeculae number *Tb.N*, trabeculae separation *Tb.Sp*, structure model index *SMI*, connectivity density *Conn.D*), or a tensor variable like mean-intercept-length-based fabric tensor (*MIL*) (Chappard et al. 2008; Zysset et al. 1998a). Furthermore, the bone tissue property can be quantitatively defined by several mechanical parameters including the tissue Young's modulus (E_t) and strength (S_t) (Wang et al. 2017). One can see that "bone quality" in the binary framework is replaced with two measurable factors, i.e., "microarchitecture" and "bone tissue property." Thus,

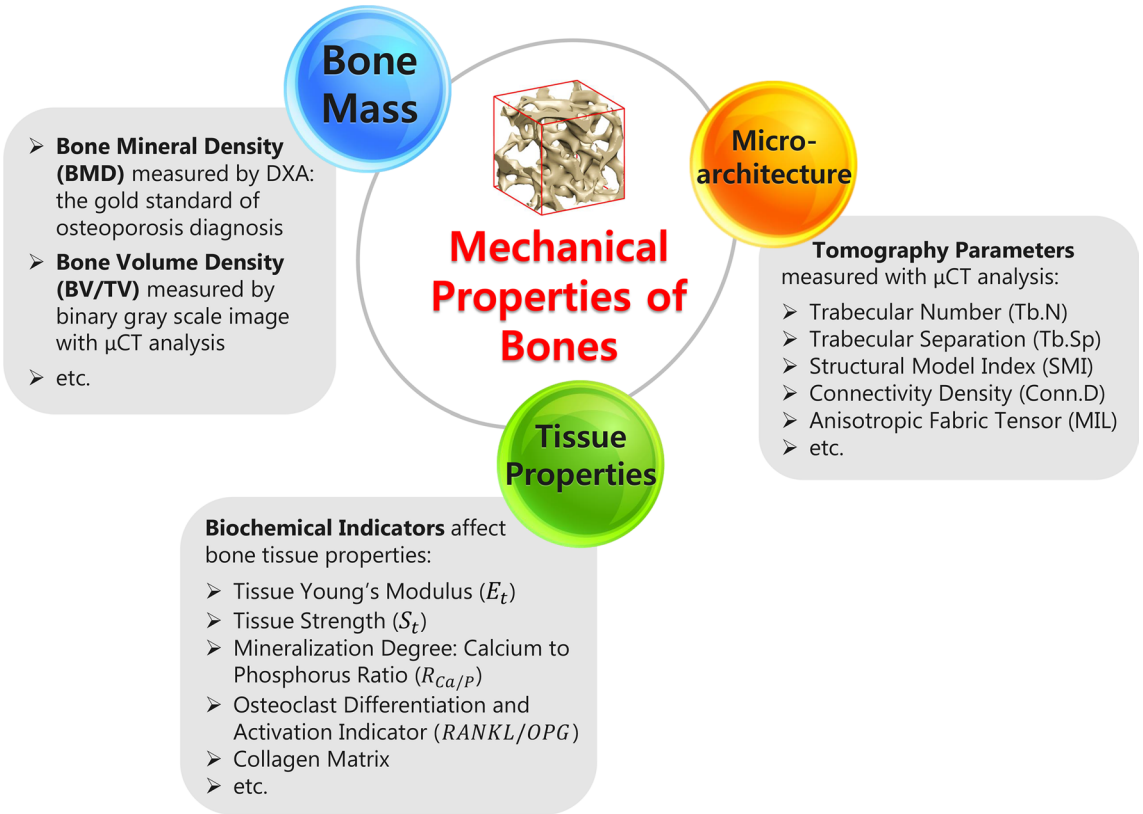

Fig. 1 The ternary framework to characterize the mechanical properties of bones

an explicit expression is possible within the ternary framework to quantify the mechanical deterioration of OP bones and can be written in a general form as follows

$$P = f\left(\text{BMD}, \text{BV/TV}, \ldots ; Tb.\text{N}, Tb.\text{Sp}, \text{SMI}, \text{Conn}.D, \text{MIL}, \ldots ; E_t, S_t, \ldots ;\right) \quad (1)$$

where P represents the apparent mechanical properties of bone such as effective Young's modulus, strength, and toughness, and f the relation functions. The effective Young's modulus with relations to bone mass, microarchitecture and tissue properties has been studied under the ternary framework in our previous work (Liu et al. 2019), but the failure properties, which are more direct and important indices measuring OP related fracture risk, have yet to be investigated. Moreover, as is seen in Eq. (1), the histomorphometric parameters and fabric tensors related to bone microarchitecture are too complex to be convenient for practical use. Thus, a crucial question arises: can we figure out one or several simple, convenient, and mechanically interpretable parameters, just like BMD and BV/TV for bone mass, to characterize the effect of microarchitecture in defining the mechanical properties of bones with different degree of OP?

It has been well recognized that the microarchitecture of cancellous bone plays a crucial role in its mechanical behaviors. The high-resolution micro-computed tomography (μCT) has greatly facilitated the microarchitecture analysis of cancellous bone (Donnelly 2011). The three-dimensional (3D) trabecular models have been rebuilt via digital modeling techniques from μCT data with higher accuracy and completeness, and, then FEM can be utilized on the 3D digital models to simulate their mechanical behaviors (Bevill and Keaveny 2009; Sandino et al. 2017). Compared to the traditional mechanical characterizations, the combination of μCT–based digital modeling and FEM simulation provides a powerful and flexible approach to explore the influence of detailed architectural features such as the aforementioned histomorphometric parameters on the mechanical properties of cancellous bones (Buie et al. 2007; Chappard et al. 2008; Karasuyama et al. 2015). Recently, Guo and his coworkers developed an individual trabecular segmentation (ITS) technique (Liu et al. 2008) and substituted individual plates and rods with shell and beam elements in FEM (Wang et al. 2013), respectively, and made the FEM simulations on microarchitectured bones more cost-efficient (Wang et al. 2015). At the mesoscale level, a second rank fabric tensor has been defined for measuring the textural and structural anisotropy for granular materials and cancellous bone (Gross et al. 2013; Turner et al. 1990). The fabric tensor can be directly related to the elastic constants of cancellous bone (Kabel et al. 1999; Van Rietbergen et al. 1998), but its relation to the failure properties has not been well established. Furthermore, the effects of microarchitecture and bone volume fraction usually mingle together in the osteoporotic samples, and their principle roles in defining the failure properties of cancellous bone are still needed to be separately clarified. It is especially worth noting again that none of these methods provide a good and convenient mechanics-based index to measure the health status of bone microarchitectures, which critically impedes clinical usage of microarchitecture information to complement BMD in OP diagnosis and treat assessment. Well filling this gap, the current paper clarified that the microarchitecture deterioration in OP bones mainly impairs their mechanical function-favorable anisotropy, termed as longitudinal superiority here, and proposed a longitudinal superiority index to quantitatively measure the health status of bone microarchitectures.

When simulating bone failure behaviors with FEM, the constitutive model of bone tissue material plays a crucial role in the accuracy and fidelity and hence attracts a lot of research attentions. Previous studies usually assumed the tissue-level elastic and yield properties based on the experimental data of cortical bones (Verhulp et al. 2008), due to the technical challenges to measure these mechanical parameters of trabecular tissue. Some simplified elastic–plastic constitutive models have been assumed for the bone tissue material and used for FEM simulations to investigate the apparent yield behaviors of cancellous bones (Harrison et al. 2013; Niebur et al. 2000). Note that all these studies provided little information about the post-yield failure process of bones, and the whole mechanical responses from elasticity, yield, softening, and up to complete failure are highly desired to determine the failure properties of bones including strength, toughness and fracture mode (Sabet et al. 2016). To this end, the continuum damage concept was incorporated into the constitutive model of bone tissue and related FEM simulations were performed for the damage initiation and progressive propagation until complete failure of cancellous bones (Hambli 2013a, 2013b; O'Connor et al. 2016; Schwiedrzik and Zysset 2013). To circumvent the convergence problem, an explicit μCT-based FEM approach was demonstrated to successfully simulate the post-yield behaviors including compacting and densification of cancellous bones (Werner et al. 2019). Different from the previous researches, the current work extracted bone tissue material parameters from the nanoscale experiment results on trabecular bones in the latest literature (Hengsberger et al. 2002; Tertuliano and Greer 2016; Zysset et al. 1998b). In particular, it remains open to debate whether OP would distinctly degrade the properties of bone tissue material. For instance, with Raman spectroscopy McCreadie et al. (McCreadie et al. 2006) examined

the chemical composition difference between healthy and OP bone tissue and stated that the OP bone tissue has a higher carbonate/amide I area ratio and carbonate/phosphate ratio, indicating the tissue degraded by OP. To the contrary, Guo and Goldstein (Guo and Goldstein 2000) utilized the nanoindentation technique to measure the elastic modulus and hardness of vertebral cancellous bone from ovariectomized rats and declared that the tissue properties are not altered by the estrogen-depletion-induced OP. However, bone tissue consists of mineral and collagen, with the former phase mainly responsible for its stiffness and strength while the latter for resilience and toughness (Fonseca et al. 2014). Therefore, aging, diabetes, osteogenesis imperfecta and other metabolic bone diseases that may cause variations in mineral, collagen or their fraction are expected to affect the mechanical properties of bone tissue (Buehler 2008; Creecy et al. 2020; Follet et al. 2004; Silva et al. 2009). With regard to this, bone tissue deterioration is definitely a concern when studying the mechanical properties of meso-/macroscopic bones.

Clarifying the separate effect of microarchitecture in OP on mechanical properties and further figuring out a convenient index measuring the microarchitecture degradation will provide novel insights into the mechanical deterioration of cancellous bones by OP and help develop novel methods for OP diagnosis and treat assessment. The current work conducted μCT-based digital modeling and FEM simulation on the cancellous bone samples acquired from healthy and ovariectomy-induced OP mice and identified the separate effects of bone mass, microarchitecture and tissue property on the failure properties of cancellous bones. Based on the results and analyses, a novel index of longitudinal superiority was put forward to mark the health status of microarchitecture of cancellous bones. The remainder of the paper is organized as follows: Sect. 2 gives details about the materials and methods; the results are discussed in Sect. 3; finally, the major conclusions are summarized in Sect. 4.

2 Materials and methods

2.1 Animal models and bone samples

The ovariectomy (OVX)-induced OP is similar in pathogenesis to that widely seen in postmenopausal women and thus usually classed into Type I osteoporosis. Eight-week-old female mice (BALB/c mouse strain) were randomly divided into two groups. One group was ovariectomized, and the other was the control group. All the mice were housed in a regulated and standard specific-pathogen-free environment (24.0 ± 0.5 C, 45–50% humidity and 12/12 h light/dark illumination cycles), with tap water and diet freely available. The animal house is under the Center for Animal Experiments, Wuhan University, in strict adherence to the AAALAC International standard for the production and usage of experimental animals. Twenty weeks after the surgery, the OVX mice were in vivo scanned by μCT to assure that the OP (strictly speaking, osteopenia here because no spontaneous fracture was observed) occurred. Then, five OVX-induced OP mice together with two healthy mice were sacrificed, and their femurs were collected as experimental specimens. All the femur specimens were fixed by 4% paraformaldehyde before scanned by a high-resolution μCT scanner for 3D digital modeling. Note that all the bone samples were taken and scanned at 28 weeks of age to avoid the age effect.

The project was approved by Institutional Animal Care and Use Committee, Wuhan University (No. 2019118). The procedures strictly complied with the National Institutes of Health Guide for the Care and Use of Laboratory Animals.

2.2 μCT scan and 3D digital modeling

The femurs were ex vivo scanned by the high-resolution μCT scanner (SkyScan 1176, Bruker, USA) at 9 μm nominal resolution with 8-bit grey level values. The X-ray source voltage and current was 45 kV and 555 μA, respectively. The μCT data were converted to 3D models with the help of the processing software Skyscan Nrecon (Bruker, USA) (Feldkamp et al. 1984) and Mimics Research (Materialise, Belgium). The calibrated grey threshold was set to differentiate the trabeculae from the background. Five cubes of volumes of interest (VOIs) with dimension $810 \times 810 \times 810$ μm were taken from the cancellous bone domain of each femur, as Fig. 2a shows. The distance between neighboring VOIs was kept at least 90 μm. To exclude cortical bones and other tissues, all the VOIs were taken from the cancellous bone domain 450 μm below the growing plate. Furthermore, the outer corners and surfaces of every VOI had been carefully checked to avoid possible inclusion of abnormally dense bones. Therefore, all the VOIs were region matched and the anatomical difference was well eliminated. Finally, 35 cubic VOIs were obtained and divided into 3 typical groups according to their BV/TV: healthy bones (10 VOIs from 2 healthy mice and the average BV/TV > 25%), mild OP bones (15 VOIs from 3 OP mice and the average BV/TV < 20%) and severe OP bones (10 VOIs from 2 OP mice and the average BV/TV < 15%), as shown in Fig. 2b. Figure 2b also shows the typical microarchitectures of the three groups of bones, where X, Y and Z axes are in the right-left, posterior-anterior and longitudinal directions of femur shaft, respectively. Comparing the three types of bones, we see that the healthy bone has a more compact structure with many plate-shaped trabeculae, while the mild OP shows a higher porosity with an increased number of rod-shaped trabeculae

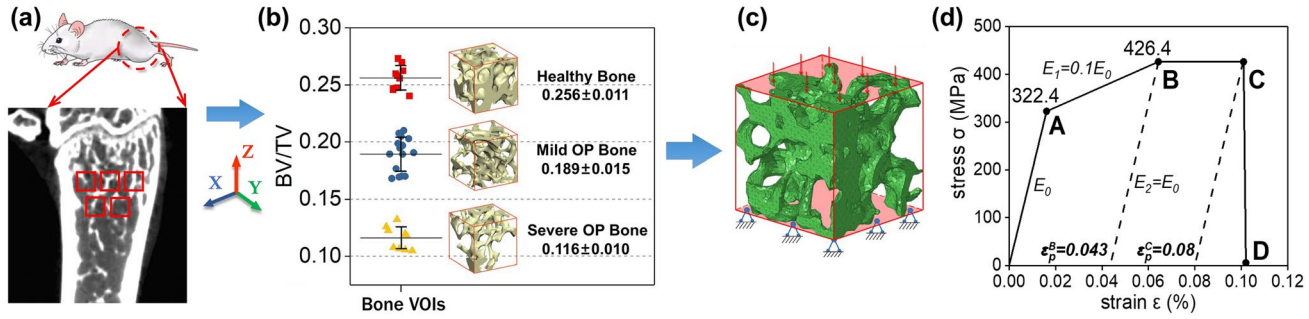

Fig. 2 Modeling procedure: (**a**) In vivo μCT scan of mice and five volume of interests (VOIs) taken from the cancellous bone domain in the distal femur samples; (**b**) all the VOIs separated into three groups according to their BV/TV: healthy, mild OP and severe OP, with the insets showing their typical 3D-microarchitectures; (**c**) an example of FEM model; (**d**) the constitutive curve of bone tissue

degraded from the plate ones, and the severe OP becomes more porous with some trabeculae absorbed.

Naturally the VOIs from different groups have quite different bone mass, microarchitecture and tissue properties simultaneously, and it is impossible to check their individual effects through direct comparisons among these natural VOIs. Therefore, we need to decouple the three factors, i.e., altering one factor while the other two fixed. Benefited from digital modeling techniques, the parameter of grey threshold can be used to alter the bone mass of the typical VOIs while keeping their microarchitecture topologies unaltered so that bone mass and microarchitecture can be decoupled. More details about the decoupled method will be discussed in Sect. 3.2. The tissue properties characterized by the material parameters such as Young's modulus, yield strength and failure strain can be manipulated in an independent way in FEM models and hence can easily be separated from bone mass and microarchitecture.

All the VOIs were meshed with C3D8 elements for FEM simulations, as shown in Fig. 2c. The element size is smaller than 8 μm compared to the 9 μm nominal resolution of μCT data, and therefore, the geometrical details of the VOIs can be well kept. Each mesh model usually has more than 1 million elements, and the mesh convergence has been guaranteed.

2.3 FEM model for mechanical simulations

FEM simulations were done on Abaqus (Dassault SIMULIA, France). An explicit approach was adopted for simulating the post-yield and damage up to complete failure behaviors in order to circumvent the convergence difficulty with the implicit approach. Nonetheless, the kinetic energy in our simulations was strictly controlled below 5% of the internal energy to reduce the dynamic effects and ensure a quasi-static loading process, and mass scaling was utilized to reduce the time cost of calculation. In Fig. 2c, a uniaxial compressive strain up to 0.2 was applied to the VOI by means of displacement control, the VOI's bottom was fully constrained, and the whole loading process until the VOI's complete failure was simulated. Uniaxial compression simulations along the X, Y and Z directions were, respectively, performed for each VOI to obtain their direction-related mechanical properties. The total loading time is about 40 s, and the corresponding strain rate is about 0.005/s, satisfying the quasi-static loading condition (strain rate typically $\leq$ 0.01/s).

Cancellous bones are network composites of trabeculae. Every individual trabecula is further composed of laminate composites where the plies of mineralized collagen fibers are mainly aligned along the longitudinal direction of trabeculae (Thurner et al. 2007). Based on the microstructural feature, it is evident that the mechanical properties of bone tissue material in trabeculae should be anisotropic with longitudinal superiority. However, the trabecular networks in mesoscale cancellous bones are irregular and complicated so that recognizing each trabecula's direction and assigning them anisotropic material properties is quite challenging, especially in the junction areas of different trabeculae. To reduce the modeling cost, the bone tissue material was assumed to be isotropic and homogeneous over all trabeculae in the current work, as usually done in the literature (Hambli 2013b; Werner et al. 2019). Its constitutive behavior can be divided into three typical stages according to Stipsitz's model (Stipsitz et al. 2020): elastic (O–A), plastic (A–B–C), and damage (C–D) until complete failure, see Fig. 2d. The element-delete technique was applied to the completely failed elements during the FEM simulations. Different from the previous researches where the tissue material properties indirectly obtained from macroscopic experiments on cortical or cancellous bone samples (Keaveny et al. 1994), the bone tissue material parameters here were based on the nanoscale experiment results on trabecular bones (Hengsberger et al. 2002; Tertuliano and Greer 2016; Zysset et al. 1998b). The initial elastic modulus (i.e., the slope of OA segment, E_0) is taken to be 20 GPa and Poisson's ratio 0.3.

Plastic deformation starts at the point A with a yield strength 322.4 MPa and linearly increases to 0.043 at the point B with a stress 426.4 MPa, correspondingly the slope of AB segment. The segment BC can be considered an ideal plastic stage. When the accumulated plastic strain reaches 0.08, the damage would initiate (Point C) and then rapidly evolve until complete failure (Point D) in a linear form of effective plastic displacement which is the product of the plastic strain and the characteristic length of mesh in FEM model.

2.4 Mechanical properties and longitudinal superiority

As mentioned in Sect. 2.2, thirty-five cubic VOIs were, respectively, taken from three groups: healthy, mild OP and severe OP bones. In FEM simulations, each VOI was uniaxially compressed by displacement loading in X, Y and Z directions, respectively, to get their apparent stress and strain at each instant by the following equations

$$\varepsilon = \frac{U}{L} \tag{2}$$

$$\sigma = \frac{F}{A} \tag{3}$$

in which U is the instant uniaxial compression displacement prescribed, L is the VOI dimension in the loading direction, F is the corresponding axial force in the loading direction, and A is the apparent area of cross section perpendicular to the loading direction. In the current paper, $L = 810\mu m$ and $A = L^2 = 810 \times 810\mu m^2$. Once the whole stress–strain curves are obtained, six mechanical parameters are defined to quantitatively characterize the elastic and failure properties of the cancellous bones in the loading direction, namely effective Young's modulus (E, the initial slope of stress–strain curve), peak strength (S, the maximum stress), peak strain (PE, the strain corresponding to the peak strength), ultimate strain (UE, the failure strain corresponding to the stress reduced to smaller than 10% of the peak strength), and toughness modulus (Γ, the area under stress–strain curve), and ultimate damage volume ratio (V_d, the volume of damage elements at ultimate strain divided by respective bone volume). Comparative studies on these mechanical parameters among healthy and OP bones can quantify the mechanical deterioration of cancellous bones due to OP.

From the perspective of functionally favorable selection and evolution of load-bearing biological materials in nature, it is well understood that a healthy microstructure of cancellous bones should be better to support their mechanical functions. In particular, since the major loadings on the bones are along their longitudinal direction, for healthy bones the longitudinal direction should be distinctly superior to its transversal directions in mechanical properties, which has been evidenced on the elastic properties in our previous study (Liu et al. 2019). Based on this, here we put forward a longitudinal superiority index to measure the health status of cancellous bone microarchitectures

$$LS(P) = \frac{P_Z}{\max\left\{P_X, P_Y\right\}} \tag{4}$$

in which P refers to some main mechanical properties such as modulus (E), strength (S) and toughness (Γ), the subscript Z is the longitudinal direction, while the X and Y are transversal directions. The corresponding LS indices are $LS(E)$ for E, $LS(S)$ for S and $LS(\Gamma)$ for Γ, etc. $LS \leq 1$ means no longitudinal superiority and the microarchitecture degraded by OP. It is especially worth noting that the mechanical longitudinal superiority of cancellous bones here purely originates from the microarchitectural topology of trabecula network, since the bone tissue material was simplified to be homogeneous and isotropic. If the longitudinal superiority at the tissue material level (i.e., individual trabecular level) is taken into consideration, one can expect that the longitudinal superiority of cancellous bones will be further enhanced.

2.5 Statistical analyses

In the following sections, the BV/TV, six mechanical properties, LS indices and so forth were usually reported as mean ± standard deviation (S.D.) for each group to well represent their average attributes. In addition, their intergroup differences were analyzed by one-way ANOVA and Tukey honestly significant difference (HSD) post hoc tests. Differences with p-value of less than 0.05 ($p < 0.05$) were considered statistically significant. In Sect. 3.2.1 and 3.2.3, quadratic fit ($\boldsymbol{y = Ax^2}$) and linear fit ($\boldsymbol{y = Ax + B}$) were performed to establish the relationship between the effective mechanical properties of cancellous bones and BV/TV, bone tissue properties, respectively. The coefficient of determination R^2 was utilized to measure the goodness of fit. All statistical analyses were performed using OriginPro 2017 software (OriginLab, USA).

2.6 3D-printed replicas and experimental verifications

3D printing as a new manufacturing technology has been demonstrated to be a novel and valuable tool for replicating and studying the complex microarchitectures of biological materials (Barak and Black 2018). Here, 3D printing was used to replicate the microarchitectures of VOIs of cancellous bones and scale up their sizes so that the conventional uniaxial compression experiments can be performed on these 3D-printed replicas. The reconstructed 3D models

of VOIs above were converted into STL format and were printed by a desktop SLA 3D printer (Form 2, Formlabs, USA) whose printing resolution can be up to 25 μm. The printing material is photopolymer resin, and the enlarged cubes are 30 × 30 × 30mm in dimension. The Young's modulus and Poisson's ratio of the photopolymer resin used for the 3D-printed models are 2.7 GPa and 0.38, respectively. Uniaxial compression experiments were conducted on a Universal Material Testing Machine (5969, Instron, USA) with displacement control. The loading and boundary conditions in the experiment were set to be the same as those in FEM simulations. A high-speed camera (FASTCAM SA5, Photron, USA) was used to record the deformation and fracture details during the loading process. Despite the material and size difference, the experimental results on the 3D-printed replicas can help qualitatively verify the FEM simulation results, especially the failure modes.

3 Results and discussion

3.1 Failure behaviors of the three types of cancellous bones

3.1.1 Characteristics of stress–strain curves

The stress–strain curves contain rich information on the intrinsic mechanical behaviors of materials. Figure 3a–c shows the typical stress–strain curves for the healthy, mild OP and severe OP bone VOIs under the loading in Z direction, respectively, in alignment with their corresponding curves of the cumulative number of damaged elements. Note that the experimental curve from the literature (Harrison et al. 2008) is also shown in Fig. 3a, and one can see that the stress–strain curve by our simulations agrees well with the experimental curve in the varying trend. Regardless of the healthy status, all the stress–strain curves experience three distinct stages: linear elastic, nonlinear plastic and stepwise damaging regimes. The linear elastic stage persists up to 1% of apparent strain, followed by the plastic stage. The transitions from the purely plastic regime to the damage regime are usually quite fast, since the cancellous bone is so porous and inhomogeneous that the stress and strain localization is likely to occur in some weak trabeculae (see the Mises stress contours Fig. S1 in Supplementary Material and the same results are reported by Harrison et al. (Harrison et al. 2008)). This can also be seen from the curves of cumulative number of damaged elements. Once there are some elements damaged, a distinct stress drop is usually seen, and the stepwise damaging regime comes into effect. The cumulative number of damaged elements stepwisely goes up with the prescribed strain, while the stress is stepwisely down in a synchronous way. The stepwise feature originated from the discontinuous failure process in cancellous bones, usually from one trabecula to another.

By comparing the curves of healthy and OP bones, we can figure out that at the same strain the stress level in the OP bones is about one order lower in magnitude than that in the healthy bones. The result is just as expected since the OP bones are abnormally porous and their stiffness and strength are greatly reduced. As the OP aggravates, the plate-like and rod-like trabeculae usually become abnormally thin, and some of the plate-like trabeculae would be converted into rod-like trabeculae while some of rod-like trabeculae may be broken and absorbed. Hence, an abnormally high proportion of rod-like trabeculae is usually seen in severe OP bones. The more porous, inhomogeneous and rod-dominant architecture of OP bones is more prone to stress concentration, buckling and bending in the slender rod-like trabeculae (see Fig. S2 in Supplementary Material , similarly observed in the experiments by Thurner et al. (Thurner et al. 2007)), and correspondingly has a larger count of trabecular rupture during the failure process. Therefore, the damage stage of

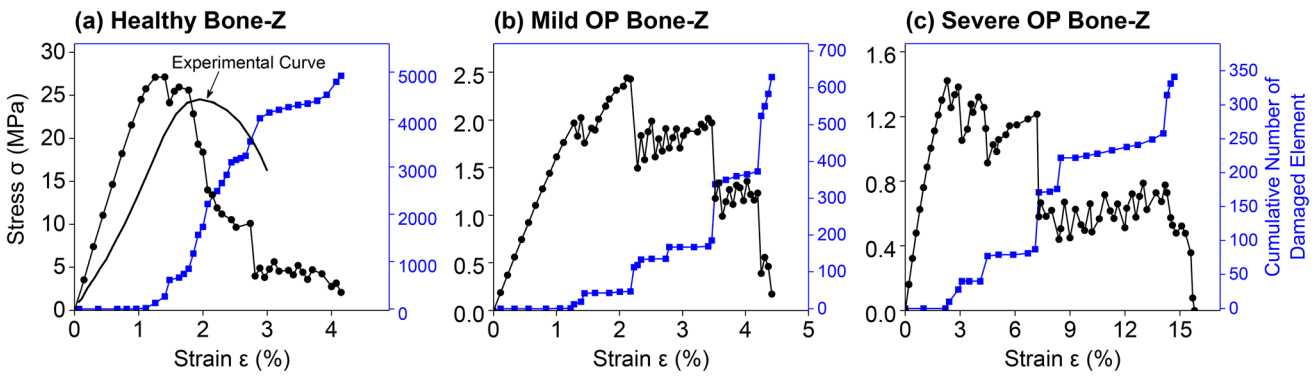

Fig. 3 Variations of stress and cumulative number of damaged element with respect to the prescribed strain: (**a**) Healthy bone (Experimental curve from Ref.(Harrison et al. 2008) included as the solid line for comparison purpose), (**b**) Mild OP bone, (**c**) Severe OP bone

OP bones tends to have more fluctuations and propagate over a larger range of strain.

3.1.2 Mechanical parameters and longitudinal superiority indices

As mentioned in Sect. 2.4, six mechanical parameters were defined based on the stress–strain curve to quantitatively characterize the elastic and failure properties of a cancellous bone sample in three orthogonal loading directions. Specifically, they are effective Young's modulus (E), peak strength (S), peak strain (PE), ultimate strain (UE), toughness modulus (Γ) and ultimate damage volume ratio (V_d). The means and standard deviations (S.D.) of the mechanical parameters for each group against the mean BV/TV are presented in the bar charts of Fig. 4, and the significant difference between any two groups is also marked by star symbol "*" (* $p<0.05$, ** $p<0.01$, *** $p<0.001$ and unmarked group is no significant difference). The detailed results of statistical analyses were shown in Table S1 in the supplementary material.

Figure 4a shows that the healthy cancellous bones have significantly higher Young's modulus in comparison with OP cancellous bones, in consistent with our previous work (Liu et al. 2019). The same conclusion can be drawn on the peak strength from Fig. 4b. Especially, the average peak strength in the Z direction is 15.55 MPa for the healthy bones and goes down to 5.31 MPa and 0.99 MPa for the mild and severe OP bones, respectively. The differences are statistically significant with $p<0.001$. Figure 4c, d shows the peak strain and ultimate strain generally increasing from the healthy bones to OP bones, but the differences between the healthy and mild OP groups are not significant. Particularly, in the Z direction, the mean values of peak strain are 0.013, 0.016 and 0.044 for the healthy, mild OP and severe OP groups, and the mean values of ultimate strain are 0.036, 0.037 and 0.078 for the three groups. Generally, the failure strain increase is due to the OP's softening effect on the cancellous bones. The softening effect may originate from two mechanisms: one is the reduction in the effective Young's modulus mainly owing to the decreased BV/TV, and the other is the premature initiation and prolongation of plastic deformation and damage process mainly attributed to the microarchitecture deterioration. The former mechanism is easily understood, and the latter mechanism is explained in the following. As the OP happens and aggravates, the cancellous bones gradually convert from the plate-trabecula dominant microstructure to the rod-trabecula

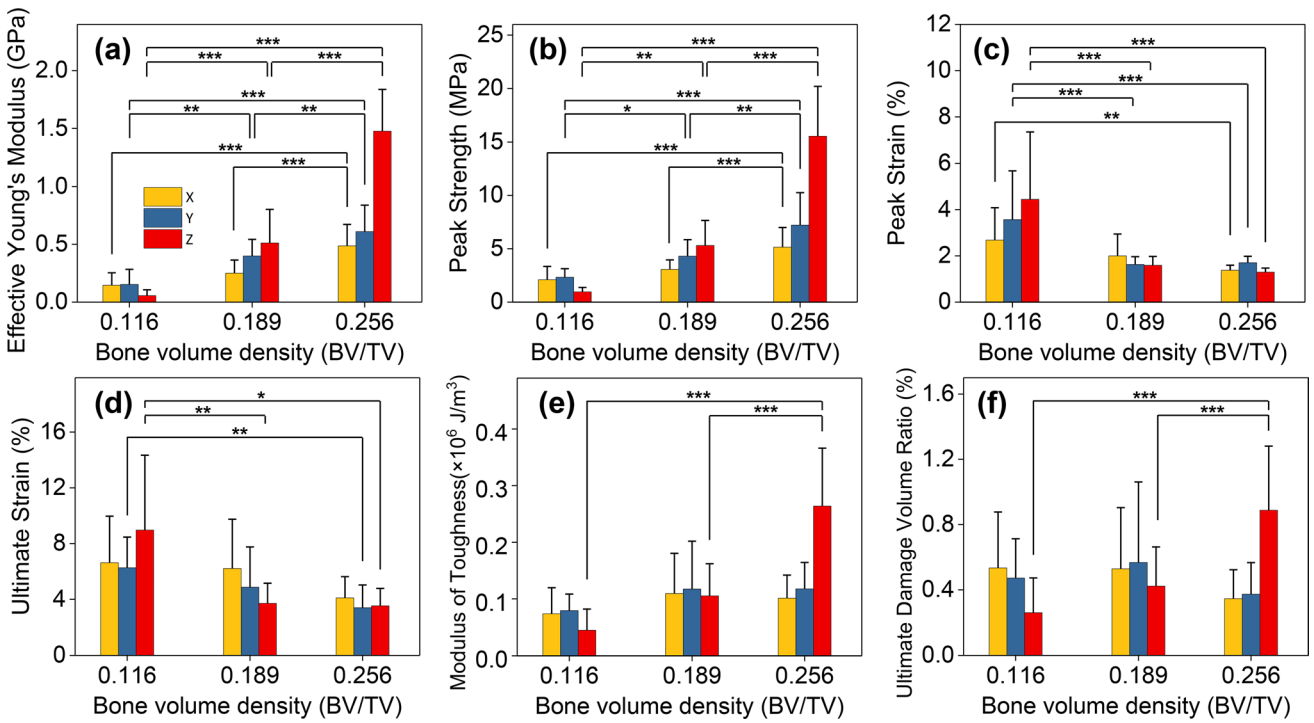

Fig. 4 Mechanical parameters obtained from statistics on the stress–strain curve of healthy bones (average BV/TV = 0.256), mild OP bones (average BV/TV = 0.189) and severe OP bones (average BV/TV = 0.116) loaded along the X, Y or Z direction: (**a**) effective Young's modulus, (**b**) peak strength, (**c**) peak strain, (**d**) ultimate strain, (**e**) Modulus of toughness and (**f**) Ultimate damage volume ratio. One-way ANOVA and Tukey HSD post hoc tests were used to study the pairwise significant difference between the healthy, mild OP and severe OP bones (* $p<0.05$, ** $p<0.01$, *** $p<0.001$). More detailed data is presented in Table S1 in the supplementary material

dominant, and the trabeculae inside become sparser, thinner and more inhomogeneous. As a result, severe stress and strain concentration (See Fig. S1) tends to happen in some trabeculae of OP VOIs, and these trabeculae are deemed to prematurely buckling (see Fig. S2), yielding and break, that in turn enhances the stress and strain concentration. Then, the trabecular buckling, yielding and damaging happen in a sequence according to their stress and strain level, and consequently, the OP VOIs tend to experience a large strain until their complete failure. This is also well evidenced by the flattened and elongated stress–strain curves in Fig. 3b, c. It is worth noting that, different from that in the effective Young's modulus and peak strength, no longitudinal superiority in the peak or ultimate strain was seen for the healthy bones. This should be attributed to the counteraction between the influences of strength and stiffness on the failure strain.

The modulus of toughness for the bones of different healthy status is shown in Fig. 4e, and the ultimate damaged volume ratio in Fig. 4f. The modulus of toughness denotes the total energy density dissipated during the whole loading process up to complete failure. As most of the energy dissipation is realized through material damage, the varying trends of toughness modulus and ultimate damaged volume ratio are similar. Especially, both of them significantly ($p<0.001$) decrease in the Z direction as OP worsens. The mean values of toughness modulus are 0.2639×10^6, 0.1053×10^6 and 0.0452×10^6 J/m^3 for the healthy, mild OP and severe OP groups, in comparison with the experimentally obtained modulus of toughness 0.2674×10^6 J/m^3 for healthy cancellous bones (Enns-Bray et al. 2018) and for 18.11×10^6 J/m^3 for the healthy bone tissue material (Tertuliano et al. 2021). The mean values of damage volume ratio are 0.89%, 0.42% and 0.26% for the three groups. The intergroup differences on tough modulus and damage volume ratio in the X and Y directions are not statistically significant ($p>0.05$). Besides, the longitudinal superiority is obvious in the healthy bones, with the mean values' ratio of toughness modulus among the X, Y and Z directions being 0.86:1:2.24 and the mean values' ratio of damaged volume ratio among the X, Y and Z directions being 0.93:1:2.38.

As mentioned above, Fig. 4 suggests that the healthy bones seem close to transversely isotropic in the mechanical properties including the effective Young's modulus, peak strength and modulus of toughness, with the longitudinal (Z direction here) properties distinctly superior to the transversal (X and Y directions here), i.e., the longitudinal superiority. To quantitatively compare the mechanical longitudinal superiority among the healthy, mild OP and severe OP bones, Fig. 5 presents the statistical analyses on the longitudinal superiority indices of the effective Young's modulus $LS(E)$, peak strength $LS(S)$ and modulus of toughness $LS(\Gamma)$, defined by Eq. (4). The detailed data can be seen in Table S2 in the supplementary material. One can see that the mean values $LS(E)=2.53$, $LS(S)=2.17$, $LS(\Gamma)=2.06$ for the healthy bones, respectively, in contrast to $LS(E)=1.30$, $LS(S)=1.28$, $LS(\Gamma)=0.84$ for the mild OP bones, and $LS(E)=0.23$, $LS(S)=0.33$ and $LS(\Gamma)=0.35$ for the severe OP bones. It can be found that the healthy bones have strong longitudinal superiority in all the three mechanical properties, with the LS indices all larger than 2. As OP happens and develops, the LS indices decrease to around 1 (mild OP) and far less than 1 (severe OP), which indicates the gradual loss of longitudinal superiority. Note that the differences of LS indices between healthy and OP groups are strongly significant ($p<0.001$). As discussed in Sect. 2.4, the longitudinal superiority should be a critical mechanical feature for healthy bones to support their major mechanical function. On the contrary, the longitudinal superiority is disrupted in OP bones, indicating that the OP disease induces the mechanical deterioration of cancellous bones in not only the magnitude but also the anisotropic feature, the former of which should be closely related to the bone loss while the latter is probably owing to the architecture alteration. The respective roles of bone mass, microarchitecture and tissue properties in defining the mechanical properties of cancellous bones will be systematically investigated and discussed in Sect. 3.2.

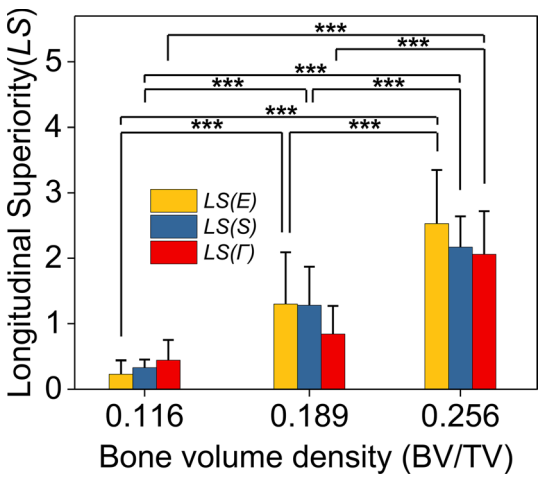

Fig. 5 The statistical analyses on the longitudinal superiority indices of the effective Young's modulus $LS(E)$, peak strength $LS(S)$ and modulus of toughness $LS(\Gamma)$ for healthy bones (average BV/TV = 0.256), mild OP bones (average BV/TV = 0.189) and severe OP bones (average BV/TV = 0.116). One-way ANOVA and Tukey HSD post hoc tests were used to study the pairwise significant difference between the healthy, mild OP and severe OP bones (* $p<0.05$, ** $p<0.01$, *** $p<0.001$)

3.1.3 Typical failure modes and experimental validation

Three typical failure modes were spotted in the FEM simulations as shown in Fig. 6a–c, and they were verified with the experimental results on the up-scaled 3D-printed replicas of bone VOIs as shown in Fig. 6d–f. The first fracture mode in Fig. 6a, d is predominant with the plate trabecula fracture and usually seen in the healthy bones because of their relatively dense microstructure and high proportion of plate trabeculae. The fracture in this mode rapidly develops from the failure initiation to completion, which is reflected as a quick drop in the stress–strain curve in Fig. 3a. The second fracture mode as shown in Fig. 6b, e is dominated by the rod trabecula fracture and frequently seen in the OP bones, particularly the severe OP bones. As OP develops, the cancellous bones become more like an inhomogeneous network of rod-like trabeculae. Under compressive loadings, the fracture in the OP bones generally begins at the weakest rod trabecula (see Figs. S1 and S2) and then jumps to the next weakest rod trabecula, propagates in a discontinuous way until the network complete failure. Compared to the first failure mode, the second failure process is usually slower and over a larger range of strain, which can be seen from the stress–strain curves in Fig. 3b, c. The third failure mode shown in Fig. 6c, f features an inclined fracture plane at the end of the failure, suggesting that the shear effect plays a prominent role during the overall propagation of failure in cancellous bones. The inclined fracture plane and underlying shear failure mechanism have been reported as well in the literature (Hambli 2013a). The highly similar failure modes seen in the experiments on the 3D-printed replicas well validate our FEM models in a qualitative way, though the 3D-printed replicas are quite different from our bone VOIs in material and size.

3.2 Respective roles of bone mass, microarchitecture and tissue properties

As mentioned in Sect. 2.2, the natural bone VOIs from different groups have different bone mass, microarchitecture and tissue properties at the same time, and thus, it is difficult to identify their separate effects through direct comparisons among them. Benefited from digital modeling techniques (Liu et al. 2019), the grey threshold was creatively used to alter the bone mass of the VOIs with their microarchitecture topologies unaltered, and thus the two factors were successfully decoupled. In addition, the tissue properties can be easily isolated from the above two with ease, since

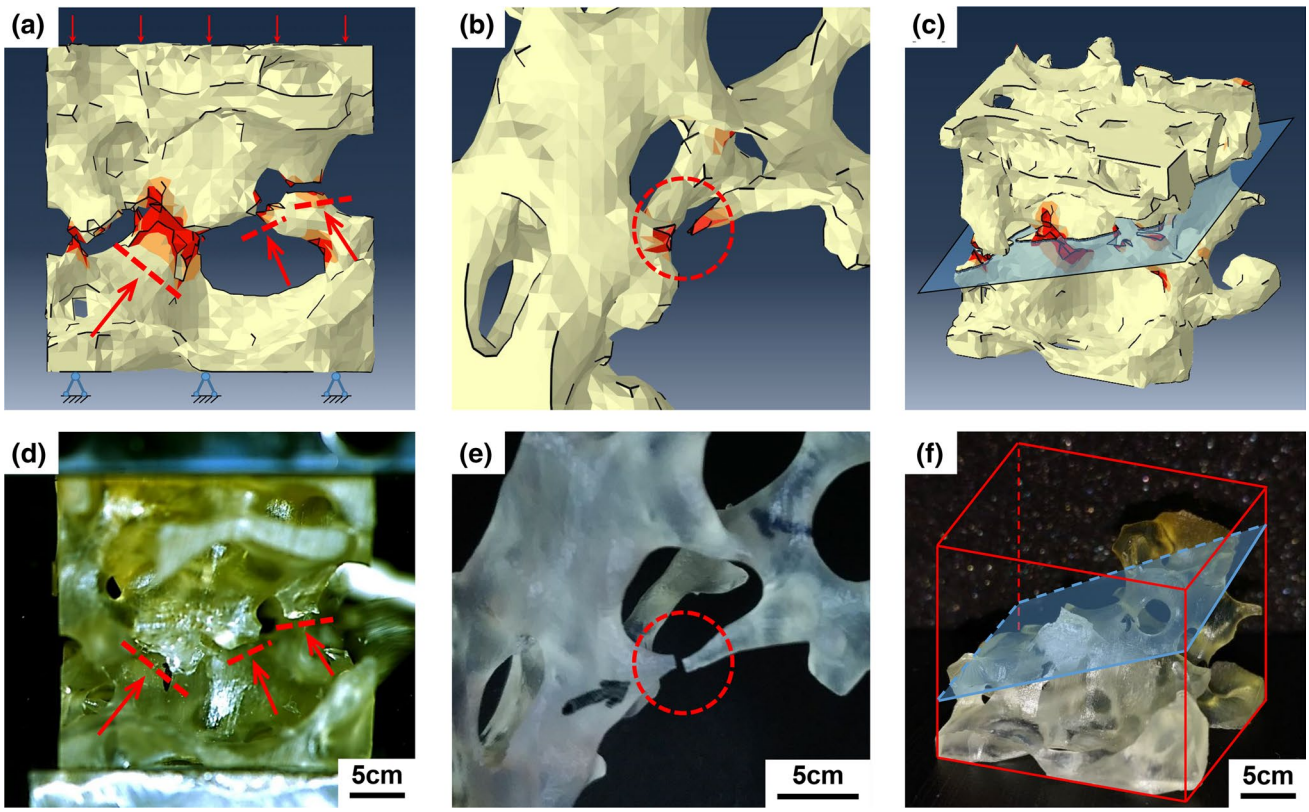

Fig. 6 The comparison of failure features between the FEM (**a–c**) and 3D-printed models (**d–f**). (**a**) and (**d**) show the plate trabecula dominant fracture, (**b**) and (**e**) the rod trabecula dominant fracture, (**c**) and (**f**) present an inclined plane of overall fracture

the material parameters such as Young's modulus, yield strength, and failure strain can be manipulated in FEM models independently.

The VOIs in gray color (yellow for online colored version) in Fig. 7 show three typical VOIs built with the calibrated grey value threshold, from the healthy, mild OP and severe OP groups, respectively. Then, the grey threshold was decently varied around the calibrated value so that the trabeculae became slightly thicker or thinner but without distinctly altering their number, and thus in the artificially generated VOIs (in dark color in Fig. 7, in light blue for online colored version) the BV/TV alteration was achieved, while the overall topological microarchitecture was well kept. Specifically, the coefficient of variation (SD/mean) for BV/TV was beyond 35%, whereas the coefficient of variation for connectivity density, structure model index and fractal dimension was limited to 15%, 14% and 4%, respectively. More detailed data are provided in Table S3 of the supplementary material. Finally, three rows of VOIs with varying BV/TV were obtained, respectively, with the healthy, mild OP, and severe OP microarchitecture, as shown in Fig. 7. Once the mechanical properties of these VOIs are acquired by FEM calculation, the BV/TV effect can be figured out by comparing the mechanical properties of the VOIs with the same microarchitecture but different BV/TV (VOIs in the same row), while the microarchitecture effect can be drawn by comparing the mechanical properties of the VOIs with the similar BV/TV but different microarchitecture (VOIs in the same column). Note that the varying range of BV/TV in each row of VOIs is between 10 and 30%, with the typical values of healthy (~25%), mild OP (~18%) and severe OP (~12%) bones well covered.

3.2.1 Individual effect of bone mass

Bone mass is definitely a significant factor determining the mechanical properties of cancellous bones. From the composites point of view, the bone volume fraction, BV/TV is a good measurement of bone mass. FEM simulations were performed to compress the VOIs in Fig. 7 along X, Y and Z directions until their complete failure, respectively. Based on the calculated stress–strain curves, the major mechanical properties such as the effective Young's modulus, peak strength and modulus of toughness for every VOI and every loading direction were determined and shown as data points against the BV/TV in Fig. 8. We can see that all the properties significantly vary with the bone volume fraction. Well-established theories have revealed that the elastic modulus and strength of cellular solids including cancellous bones usually vary as a power function of BV/TV, $\boldsymbol{y} = \boldsymbol{A}\boldsymbol{x}^{\boldsymbol{\beta}}$, with $\boldsymbol{y}$ and $\boldsymbol{x}$ denoting the mechanical properties and BV/TV, respectively, $\boldsymbol{A}$ a coefficient to be determined by fitting, and the exponent $\boldsymbol{\beta}$ usually ranging from 1 to 3 (Currey 1986; Gibson 2005; Morgan et al. 2003). For stochastic foams such as cancellous bones, $\boldsymbol{\beta}$=2 is suggested in the textbook (Gibson 2003). Hence, the quadratic function $\boldsymbol{y} = \boldsymbol{A}\boldsymbol{x}^2$ was used to fit the data in Fig. 8a–i, respectively. The fitting plots are presented as solid lines in Fig. 8 for different microarchitectures and different directions, and the corresponding fitting coefficients $\boldsymbol{A}$ are listed in Table 1. It can be clearly seen

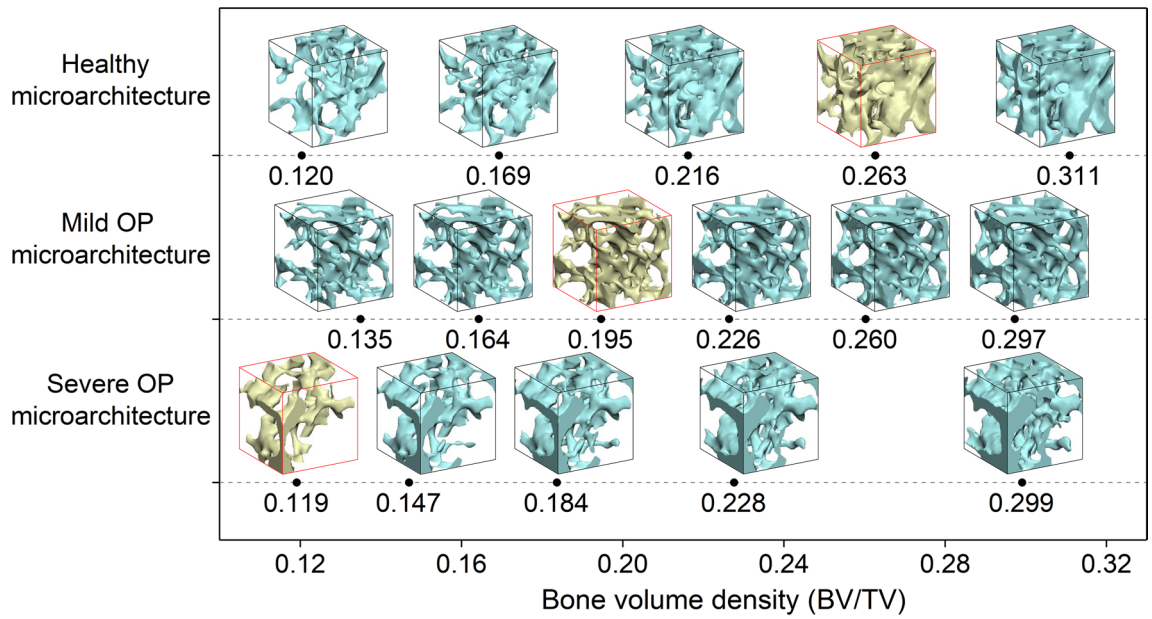

Fig. 7 A variety of bone volume densities acquired for three typical microarchitectures (healthy, mild OP, and severe OP) through in silico altering the threshold of relative grey value. (Adapted from Ref.(Liu et al. 2019))

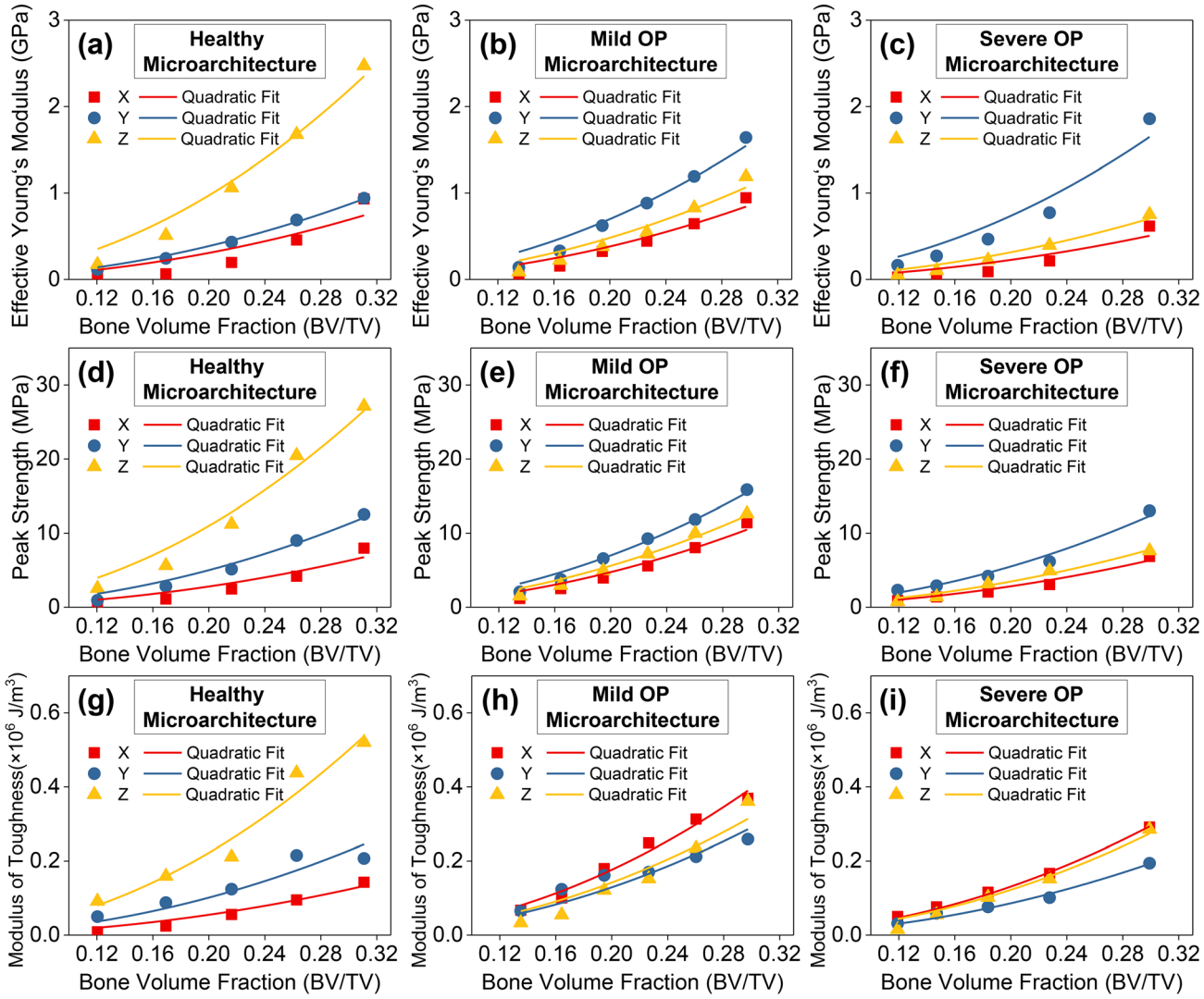

Fig. 8 The mechanical properties varying against the bone volume fraction for the three typical bone microarchitectures: healthy, mild OP and severe OP. (**a–c**) The effective Young's modulus, (**d–f**) peak strength and (**g–i**) modulus of toughness. The curves are from fitting a quadratic function $\boldsymbol{y} = \boldsymbol{A}\boldsymbol{x}^2$ to the simulations results

that the quadratic function can well describe the variations of effective Young's modulus, peak strength and modulus of toughness with the bone volume fraction for all types of microarchitectures and all loading directions, with the coefficient of determination $\boldsymbol{R}^2$ all greater than 0.80, in most of situations even beyond 0.95, see Table 1. The quadratic dependence of the elastic and failure properties of cancellous bones on the bone volume fraction strongly suggests that bone mass is one of the most prominent factors governing the bone mechanical properties regardless of bone microarchitecture and loading direction.

Now let us make a comparison among the healthy, mild OP, and severe OP microarchitectures. For the healthy microarchitecture, we can see from Fig. 8a, d, g that the curves of Z direction are always above those of X and Y directions, indicating that the effective stiffness, strength and toughness of healthy microarchitectured bones always exhibit the longitudinal superiority. The conclusion can also be drawn from the longitudinal superiority (LS^*) in Table 1, calculated from the coefficients $\boldsymbol{A}$ of different directions. In particular, the longitudinal superiority estimated by $LS^* = A_Z / \max\{A_X, A_Y\}$=2.52 for the effective Young's modulus, 2.19 for the peak strength and 2.19 for the modulus of toughness. The coefficient $\boldsymbol{A}$ of the longitudinal (Z) direction is at least two folds higher than that of the transverse directions (X and Y). All these again suggest that the healthy microstructured cancellous bone exhibits significant longitudinal superiority in terms of both elastic

Table 1 The fitted coefficient (A) of property-density function $y = Ax^2$ and corresponding coefficient of determination (R^2) for the three typical trabecular bone microarchitectures. The longitudinal superiority (LS^*) calculated from the coefficients also listed

		Effective young's modulus		Peak strength		Modulus of toughness	
		A	R^2	A	R^2	A	R^2
Healthy microarchitecture	X	7.68	0.82	69.97	0.90	1.37	0.96
	Y	9.66	0.99	125.2	0.98	2.54	0.83
	Z	24.33	0.97	274.6	0.97	5.56	0.96
LS^*: $A_Z/\max(A_X, A_Y)$		2.52		2.19		2.19	
Mild OP microarchitecture	X	9.55	0.92	118.6	0.96	4.41	0.97
	Y	17.47	0.96	175.0	0.98	3.23	0.84
	Z	12.06	0.94	140.0	0.98	3.55	0.92
LS^*: $A_Z/\max(A_X, A_Y)$		0.69		0.80		0.81	
Severe OP microarchitecture	X	5.66	0.84	70.69	0.97	3.28	0.99
	Y	18.42	0.93	137.7	0.98	2.15	0.98
	Z	7.87	0.96	86.82	0.98	3.06	0.98
LS^*: $A_Z/\max(A_X, A_Y)$		0.43		0.63		0.93	

and failure properties. For the mild OP microarchitecture (see Fig. 8b, e, h), the longitudinal curve is lowered to be sandwiched by the transverse curves, and the coefficient A_Z is also decreased to be between A_X and A_Y, particularly, $LS^*(E) = 0.69$, $LS^*(S) = 0.80$ and $LS^*(\Gamma) = 0.81$ (see Table 1). This tells us that the function-favorable longitudinal superiority has been ruined by the OP microarchitecture whatever the BV/TV varies. The same trend can be figured out for the severe OP microarchitecture (see Fig. 8c, f, i). With the OP microarchitectures, increasing BV/TV tends to enhance one of the transverse directions (e.g., Y) instead of the major physiological loading direction Z. Moreover, the OP microarchitectures still give distinctly poorer mechanical properties than the healthy one even when their BV/TV is recovered to the healthy level (about 0.25 here), especially in the major physiological loading direction Z. A great implication for OP treatment in clinics can be inferred that sole recovery of bone mass cannot guarantee the mechanical property recovery of OP bones. Actually, some OP medical treatments (e.g., alendronate) have been reported able to increase bone mass but fail to improve bone microstructure accordingly (Rizzoli et al. 2010).

3.2.2 Individual effect of microarchitecture

As is aforementioned that the microarchitecture is an important aspect concerning the mechanical properties of cancellous bones, this section is dedicated to studying its individual role decoupled from the bone mass. The above analyses in Fig. 8 have suggested that the anisotropic characteristics of the effective Young's modulus, peak strength and modulus of toughness are closely related to the types of microarchitecture. It implies that the microarchitecture plays a dominant role in defining the anisotropic feature of the mechanical properties of cancellous bones. To better illustrate this point, the longitudinal superiority indices of effective modulus, peak strength, and modulus of toughness for the healthy, mild OP and severe OP microarchitectures are shown in Fig. 9, with the central data point as the mean value, the error bar as the standard deviation, and the star data points calculated from the fitted coefficients in Table 1 are also included for reference. The detailed statistical data can be seen in Table S4 in the supplementary material. The LS indices of healthy and OP bones have significant difference. For the healthy microarchitecture, the mean values of longitudinal superiority

$$LS(E) = 2.22, LS(S) = 2.26, LS(\Gamma) = 1.98 \tag{5}$$

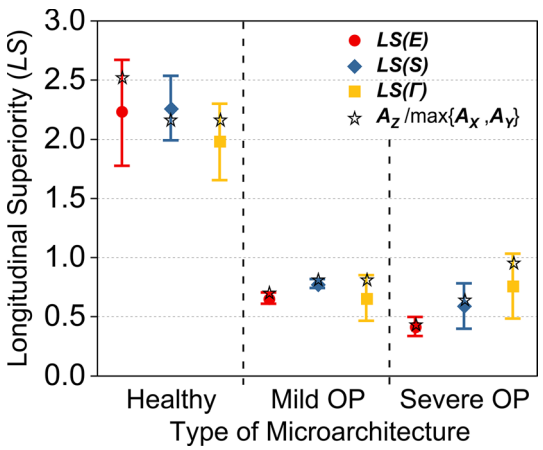

Fig. 9 The longitudinal superiority indices with the effective modulus, peak strength and modulus of toughness of healthy, mild OP and severe OP microstructured bones. The center data points denote the mean values, the error bars are the standard deviations, and the hallow stars are calculated from the fitting coefficients in Table 1

all of which are significantly greater than one. All these clearly demonstrate that the healthy microarchitecture owns an anisotropic feature of longitudinal superiority not only in the elastic property (effective Young's modulus) but also in the failure properties (peak strength and toughness modulus). The longitudinal superiority fits well with the mechanical function of long bones, since the major physiological loadings in daily life are usually in their longitudinal direction. Hence, the longitudinal superiority can be considered as a key feature of healthy bone microstructures. For the mild OP microarchitecture,

$$LS(E) = 0.66, LS(S) = 0.78, LS(\Gamma) = 0.66 \tag{6}$$

and for the severe OP microarchitecture,

$$LS(E) = 0.42, LS(S) = 0.59, LS(\Gamma) = 0.76 \tag{7}$$

all of them are significantly less than one. The same trend can also be seen from LS^* for the healthy and OP microstructured bones. One can conclude that the longitudinal mechanical properties are reduced out of proportion to their transverse counterparts in the OP bones, and the longitudinal superiority does not hold anymore within the OP microarchitectures. The loss of longitudinal superiority would lead to the mismatch between the superior direction of mechanical properties and the major direction of physiological loadings, which is the OP-induced critical deterioration to the microarchitecture of cancellous bones.

3.2.3 Individual effect of tissue property

Bone tissue material mainly consists of mineralized collagen nanofibers. The degree of mineralization and the elasticity and resilience of collagen are inclined to be affected by aging and some skeletal diseases including OP. Correspondingly, the elastic modulus, yield stress, strength (maximum stress) and ultimate strain in the standard stress–strain curve (see Fig. 2c) would be changed (Follet et al. 2004; Launey et al. 2010). In order to systematically investigate how different variations of bone tissue affect the mechanical properties of cancellous bone, two types of variations on the standard constitutive curve are designed to simulate the degradation of mineral and collagen, respectively, as shown in Fig. 10a, b. In Fig. 10a, the tissue strength (S_t) varies linearly at 10% intervals around the standard strength 426.4 MPa, while the tissue moduli E_0 and E_1, the plastic strain (ε_p^B=0.043) and the ultimate strain ($\varepsilon^u = 0.101$) are kept as constants. In Fig. 10b, the ultimate strain ε^u is linearly altered around the standard value 0.101, whereas the moduli E_0 and E_1 and the tissue strength S_t are kept unchanged. These constitutive curves were input to FEM models to calculate the mechanical properties of the typical VOIs. Note that the variation of tissue stiffness (E_0) was not considered here, since it has been done in our previous work (Liu et al. 2019) and showed that the variation of tissue stiffness has a linear and mild influence on the effective stiffness of cancellous bones.

The computational results of peak strength are plotted against the percentage variation of tissue strength S_t (solid points) and ultimate strain ε^u (blank points) in Fig. 11a–c, respectively, for the healthy, mild OP and severe OP bones. The results of modulus of toughness are similarly shown in Fig. 11d–f. The lines (solid for the tissue strength variation and dash for the ultimate plastic variation) are given by fitting a linear function $\boldsymbol{y} = \boldsymbol{Ax} + \boldsymbol{B}$ to the simulation data, in which $\boldsymbol{y}$ and $\boldsymbol{x}$ respectively refer to the mechanical properties (peak strength and modulus of toughness) of cancellous bones and the bone tissue properties (strength and ultimate strain). The coefficient $\boldsymbol{A}$ and coefficient of determination $\boldsymbol{R}^2$ are shown in Table 2, and the most of $\boldsymbol{R}^2$ are greater than 0.9, indicating that the linear function fits the data very well. Thus, it can be concluded that the failure properties of cancellous bones such as the peak strength and toughness

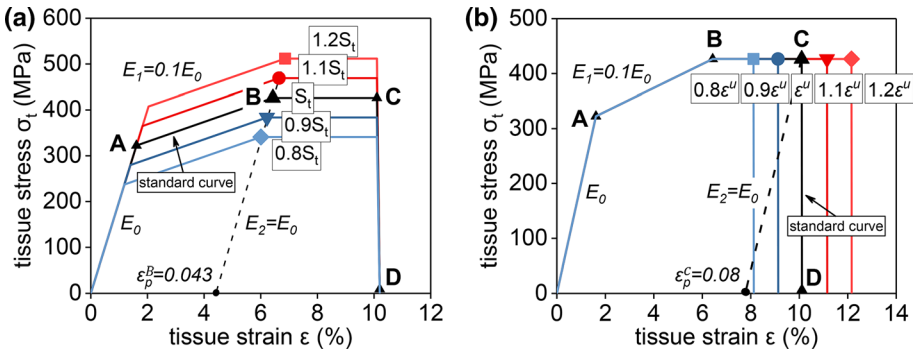

Fig. 10 Two types of change to the constitutive curve of bone tissue: **(a)** linearly varying the tissue strength (S_t) with the moduli (E_0, E_1) and the plastic strain (ε_p^B) fixed, **(b)** linearly varying the ultimate strain (ε^u) with the moduli (E_0, E_1) and tissue strength (S_t) unaltered. The varying range is from − 20 to 20% around the standard value at 10% intervals. The former is mainly designed to simulate the change in biomineral whereas the latter the change in collagenous matrix

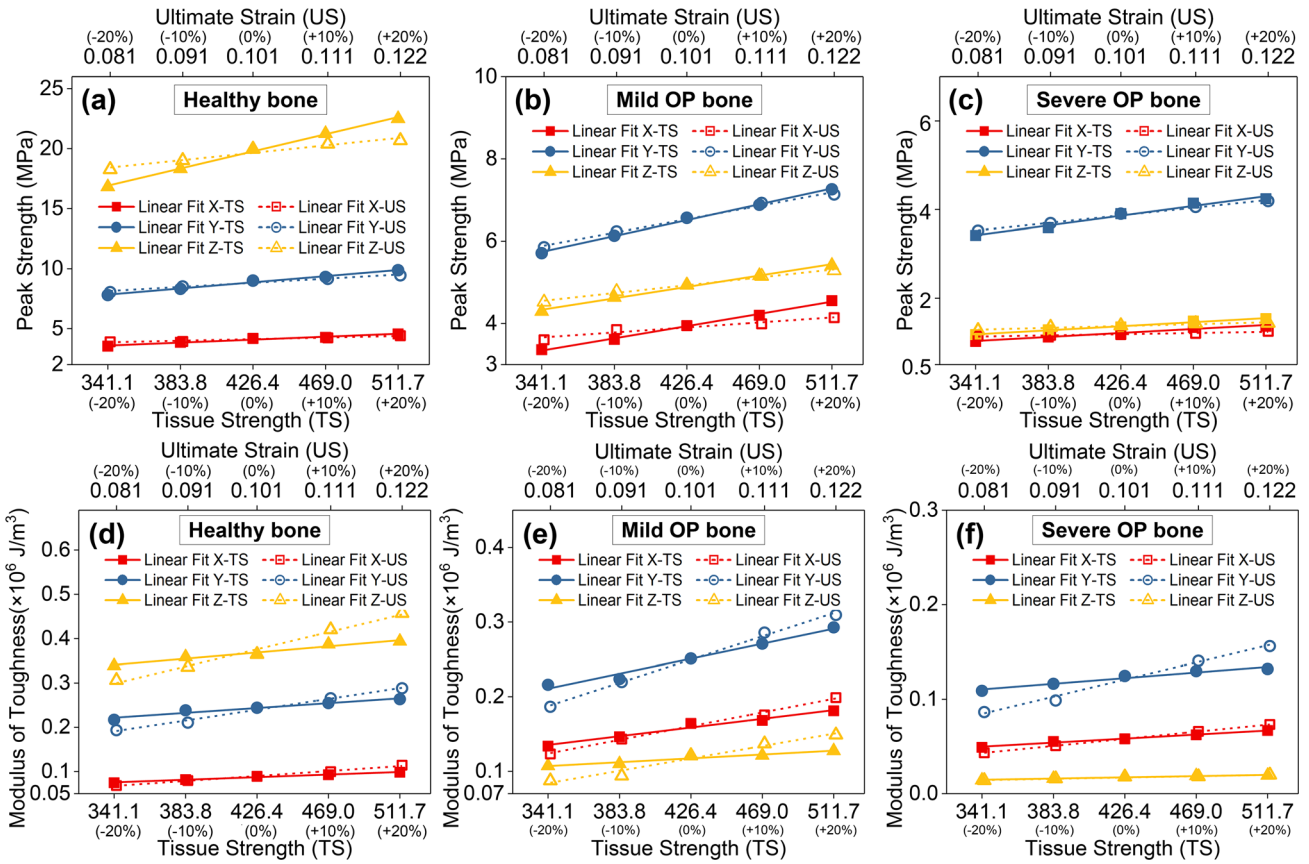

Fig. 11 The failure properties varying against the tissue properties. The peak strength with respect to the tissue strength (solid points and lines) and ultimate strain (blank data points and dash lines) for the healthy bone (**a**), mild OP bone (**b**), and severe OP bone (**c**). The modulus of toughness against the tissue strength and ultimate strain for the healthy bone (**d**), mild OP bone (**e**), and severe OP bone (**f**). The lines are linear fitting to the simulation data

Table 2 The coefficient (A) of function $y = Ax + B$ and coefficient of determination (R^2) for the relations between mechanical properties (y) and tissue properties (x) with the three typical trabecular bone microarchitectures. The longitudinal superiority (LS^*) calculated from the coefficients also listed

		Peak strength				Modulus of toughness			
		Tissue strength		Ultimate strain		Tissue strength		Ultimate strain	
		$A\times10^{-2}$	R^2	A	R^2	$A\times10^{-2}$	R^2	A	R^2
Healthy bone	X	0.58	0.97	13.06	0.92	0.014	0.98	1.11	0.99
	Y	1.20	0.98	34.08	0.94	0.026	0.94	2.42	0.98
	Z	3.35	0.99	61.44	0.94	0.033	0.95	3.83	0.98
LS^*:$A_Z/\max(A_X, A_Y)$		2.79		1.80		1.27		1.58	
Mild OP bone	X	0.70	0.99	12.05	0.91	0.027	0.96	1.82	0.99
	Y	0.90	0.99	32.18	0.99	0.047	0.97	3.08	0.99
	Z	0.65	0.99	18.84	0.98	0.012	0.93	1.64	0.96
LS^*:$A_Z/\max(A_X, A_Y)$		0.72		0.59		0.26		0.53	
Severe OP bone	X	0.21	0.96	2.64	0.95	0.010	0.99	0.74	0.99
	Y	0.52	0.97	16.89	0.99	0.014	0.95	1.79	0.98
	Z	0.22	0.98	4.11	0.92	0.003	0.94	0.14	0.94
LS^*:$A_Z/\max(A_X, A_Y)$		0.42		0.24		0.21		0.078	

modulus are positively and linearly related to the tissue properties such as strength S_t and ultimate strain ε^u, with analogy to the previously reported relation of bone modulus to the tissue modulus (Liu et al. 2019).

In Fig. 11a–c, the slopes of the solid lines are slightly larger than those of the dash lines, whereas the trend is reversed in Fig. 11d–f. The trends tell that the peak strength of cancellous bones is more sensitive to the tissue strength, while the modulus of toughness of cancellous bones is more sensitive to the ultimate strain of bone tissue. It is quite understandable since at the tissue level the ultimate strain is a parameter more related to the modulus of toughness than the strength. For the healthy bone, the lines of the peak strength and modulus of toughness for Z direction are always on the top, those for X direction are always on the bottom, while those for Y direction are between them, see Fig. 11a, d. This indicates that the critical anisotropic feature, longitudinal superiority persists well with the healthy bones irrespective of the variations of tissue properties. For the mild and severe OP bones, the lines for Z direction are not on the top any more, but the relative positions of the lines for different directions are still unaltered as the tissue properties vary, see Fig. 11b–c, e–f. Therefore, it can be inferred that the mechanical anisotropy of cancellous bones is mainly defined by their microarchitectures, and the healthy microarchitectures clearly exhibit longitudinal superiority well adapted to their mechanical functions. The same conclusion can also be drawn from the longitudinal superiority (LS^*) in Table 2, calculated from the coefficients $\boldsymbol{A}$ of different directions. Moreover, if the tissue strength S_t is reduced by 20%, the peak strength of healthy bone in Z direction decreases about 15.8%, from 19.96 MPa to 16.81 MPa, which is still much larger than its counterparts of mild (4.94 MPa) and severe (1.35 MPa) OP bones with the standard tissue properties. If the ultimate strain ε^u is reduced by 20%, the modulus of toughness of healthy bone in Z direction decreases about 15.97%, from 364,350 to 306,180 J/m^3, which is still much larger than its counterparts of mild (121,330 J/m^3) and severe (17,850 J/m^3) OP bones with the standard tissue properties. These comparisons suggest that the negative impact of tissue property degradation may not be as significant as bone loss and microarchitecture deterioration in OP.

4 Summary

Although it has been well recognized that besides bone loss, microarchitecture degradation plays a crucial role in the mechanical deterioration of OP bones, the specific role of microarchitecture in OP has not been well clarified and quantified. In the paper, the OVX mice were utilized to establish the animal models of type I OP, and μCT-based digital modeling and FEM simulations were conducted to identify the decoupled and individual roles of bone mass, microarchitecture and tissue property in the mechanical deterioration of OP bones under the ternary composite framework. The major findings and conclusions are summarized as follows:

(1) Compared to the OP bones, healthy bones have not only a larger bone volume fraction but also a function-favorable microarchitecture and thus give a higher stiffness, strength, toughness, and especially the longitudinal superiority in all these major mechanical properties. The longitudinal superiority of healthy bones is a critical anisotropic feature well matching to their mechanical functions. A longitudinal superiority index was defined as the ratio of longitudinal mechanical properties over their transverse counterparts to measure the health status of bone microarchitectures.

(2) The respective effects of bone mass, microarchitecture and tissue material are summarized in Fig. 12. Bone mass has a major influence on the magnitude of effective stiffness, strength and toughness of cancellous bones, with a quadratic relation ($\boldsymbol{y = Ax^2}$). Microarchitecture critically defines their anisotropic features. Tissue properties only have a mild influence on their magnitudes, with a linear relation ($\boldsymbol{y = Ax + B}$).

(3) While BMD and BV/TV are well accepted and used as indices of bone mass, there still lacks good and convenient indices for microarchitecture. Besides the well-known bone loss, we found that the microarchitecture-deterioration-induced directional mismatch between material and loading is another distinct feature of OP, and hence the longitudinal superiority index was defined as a measurement of the health status of can-

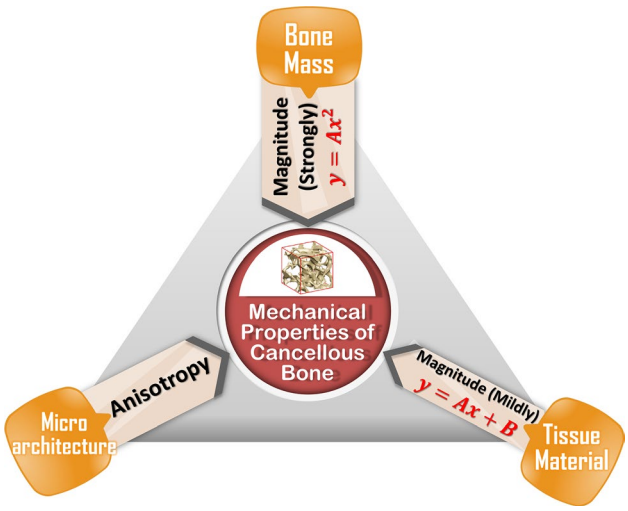

Fig. 12 The decoupled effects of bone mass, microarchitecture and tissue properties on the mechanical properties of cancellous bone

cellous bone microarchitecture, with its value significantly larger than one indicating healthy and otherwise unhealthy.

Supplementary Information The online version contains supplementary material available at https://doi.org/10.1007/s10237-021-01491-z.

Acknowledgements Our thanks are due to Prof. Huajian Gao, Bin Liu, Dr. Qifang Yin and Mr. Kun Geng for their valuable suggestions. The work was supported by National Natural Science Foundation of China (Grant Nos. 11772240, 11720101002, 11542001, 11502175), Jiangsu Natural Science Foundation (Grant No. BK20150381), the Fundamental Research Funds for the Central University, Translational Medicine and Interdisciplinary Research Joint Fund of Zhongnan Hospital of Wuhan University (Grant No. ZNJC201927) and the Innovative Group Development Program at School of Civil Engineering, Wuhan University.

Declarations

Conflict of interest The authors declare that they have no conflict of interest

References

Barak MM, Black MA (2018) A novel use of 3D printing model demonstrates the effects of deteriorated trabecular bone structure on bone stiffness and strength. J Mech Behav Biomed 78:455–464. https://doi.org/10.1016/j.jmbbm.2017.12.010

Becker DJ, Kilgore ML, Morrisey MA (2010) The societal burden of osteoporosis. Curr Rheumatol Rep 12:186–191

Bevill G, Keaveny TM (2009) Trabecular bone strength predictions using finite element analysis of micro-scale images at limited spatial resolution. Bone 44:579–584. https://doi.org/10.1016/j.bone.2008.11.020

Buehler MJ (2008) Nanomechanics of collagen fibrils under varying cross-link densities: Atomistic and continuum studies. J Mech Behav Biomed 1:59–67. https://doi.org/10.1016/j.jmbbm.2007.04.001

Buie HR, Campbell GM, Klinck RJ, MacNeil JA, Boyd SK (2007) Automatic segmentation of cortical and trabecular compartments based on a dual threshold technique for in vivo micro-CT bone analysis. Bone 41:505–515. https://doi.org/10.1016/j.bone.2007.07.007

Chappard D, Baslé M-F, Legrand E, Audran M (2008) Trabecular bone microarchitecture: a review. Morphologie 92:162–170

Ciarelli TE, Fyhrie DP, Schaffler MB, Goldstein SA (2000) Variations in three-dimensional cancellous bone architecture of the proximal femur in female hip fractures and in controls. J Bone Miner Res 15:32–40. https://doi.org/10.1359/jbmr.2000.15.1.32

Creecy A et al (2020) The age-related decrease in material properties of BALB/c mouse long bones involves alterations to the extracellular matrix. Bone 130:115126

Cummings SR, Karpf DB, Harris F, Genant HK, Ensrud K, LaCroix AZ, Black DM (2002) Improvement in spine bone density and reduction in risk of vertebral fractures during treatment with antiresorptive drugs. Am J Med 112:281–289. https://doi.org/10.1016/S0002-9343(01)01124-X

Currey JD (1986) Power law models for the mechanical properties of cancellous bone. Eng Med 15:153–154

Delmas PD, Seeman E (2004) Changes in bone mineral density explain little of the reduction in vertebral or nonvertebral fracture risk with anti-resorptive therapy. Bone 34:599–604. https://doi.org/10.1016/j.bone.2003.12.022

Donnelly E (2011) Methods for assessing bone quality: a review. Clin Orthop Relat R 469:2128–2138. https://doi.org/10.1007/s11999-010-1702-0

Enns-Bray WS, Ferguson SJ, Helgason B (2018) Strain rate dependency of bovine trabecular bone under impact loading at sideways fall velocity. J Biomech 75:46–52. https://doi.org/10.1016/j.jbiomech.2018.04.042

Feldkamp LA, Davis LC, Kress JW (1984) Practical cone-beam algorithm. Josa A 1:612–619

Follet H, Boivin G, Rumelhart C, Meunier PJ (2004) The degree of mineralization is a determinant of bone strength: a study on human calcanei. Bone 34:783–789. https://doi.org/10.1016/j.bone.2003.12.012

Fonseca H, Moreira-Goncalves D, Coriolano HJA, Duarte JA (2014) Bone quality: the determinants of bone strength and fragility. Sports Med 44:37–53. https://doi.org/10.1007/s40279-013-0100-7

Gibson LJ (2003) Cellular solids. Mrs. Bulletin 28:270–274

Gibson LJ (2005) Biomechanics of cellular solids. J Biomech 38:377–399. https://doi.org/10.1016/j.jbiomech.2004.09.027

Gross T, Pahr DH, Zysset PK (2013) Morphology-elasticity relationships using decreasing fabric information of human trabecular bone from three major anatomical locations. Biomech Model Mechan 12:793–800. https://doi.org/10.1007/s10237-012-0443-2

Guo XE, Goldstein SA (2000) Vertebral trabecular bone microscopic tissue elastic modulus and hardness do not change in ovariectomized rats. J Orthop Res 18:333–336

Hambli R (2013a) Micro-CT finite element model and experimental validation of trabecular bone damage and fracture. Bone 56:363–374. https://doi.org/10.1016/j.bone.2013.06.028

Hambli R (2013b) A quasi-brittle continuum damage finite element model of the human proximal femur based on element deletion. Med Biol Eng Comput 51:219–231. https://doi.org/10.1007/s11517-012-0986-5

Hambli R, Bettamer A, Allaoui S (2012) Finite element prediction of proximal femur fracture pattern based on orthotropic behaviour law coupled to quasi-brittle damage. Med Eng Phys 34:202–210. https://doi.org/10.1016/j.medengphy.2011.07.011

Harrison NM, McDonnell PF, O'Mahoney DC, Kennedy OD, O'Brien FJ, McHugh PE (2008) Heterogeneous linear elastic trabecular bone modelling using micro-CT attenuation data and experimentally measured heterogeneous tissue properties. J Biomech 41:2589–2596. https://doi.org/10.1016/j.jbiomech.2008.05.014

Harrison NM, McDonnell P, Mullins L, Wilson N, O'Mahoney D, McHugh PE (2013) Failure modelling of trabecular bone using a non-linear combined damage and fracture voxel finite element approach. Biomech Model Mechan 12:225–241. https://doi.org/10.1007/s10237-012-0394-7

Hengsberger S, Kulik A, Zysset P (2002) Nanoindentation discriminates the elastic properties of individual human bone lamellae under dry and physiological conditions. Bone 30:178–184. https://doi.org/10.1016/S8756-3282(01)00624-X

Homminga J, McCreadie BR, Ciarelli TE, Weinans H, Goldstein SA, Huiskes R (2002) Cancellous bone mechanical properties from normals and patients with hip fractures differ on the structure level, not on the bone hard tissue level. Bone 30:759–764. https://doi.org/10.1016/S8756-3282(02)00693-2

Jordan GR et al (2003) Increased femoral neck cancellous bone and connectivity in coxarthrosis (hip osteoarthritis). Bone 32:86–95. https://doi.org/10.1016/S8756-3282(02)00920-1

Kabel J, van Rietbergen B, Odgaard A, Huiskes R (1999) Constitutive relationships of fabric, density, and elastic properties in cancellous

bone architecture. Bone 25:481–486. https://doi.org/10.1016/S8756-3282(99)00190-8
Karasuyama K, Yamamoto T, Motomura G, Sonoda K, Kubo Y, Iwamoto Y (2015) The role of sclerotic changes in the starting mechanisms of collapse: a histomorphometric and FEM study on the femoral head of osteonecrosis. Bone 81:644–648. https://doi.org/10.1016/j.bone.2015.09.009
Keaveny TM, Guo XE, Wachtel EF, Mcmahon TA, Hayes WC (1994) Trabecular bone exhibits fully linear elastic behavior and yields at low strains. J Biomech 27:1127–1136. https://doi.org/10.1016/0021-9290(94)90053-1
Keaveny TM, Morgan EF, Niebur GL, Yeh OC (2001) Biomechanics of trabecular bone. Annu Rev Biomed Eng 3:307–333. https://doi.org/10.1146/annurev.bioeng.3.1.307
Launey ME, Buehler MJ, Ritchie RO (2010) On the Mechanistic origins of toughness in bone. Annu Rev Mater Res 40:25–53. https://doi.org/10.1146/annurev-matsci-070909-104427
Licata A (2009) Bone density versus bone quality: What's a clinician to do? Clev Clin J Med 76:331–336
Lin JT, Lane JM (2004) Osteoporosis–a review. Clin Orthop Relat R 27:126–134. https://doi.org/10.1097/01.blo.0000132404.30139.f2
Liu P, Liang X, Li Z, Zhu X, Zhang Z, Cai L (2019) Decoupled effects of bone mass, microarchitecture and tissue property on the mechanical deterioration of osteoporotic bones. Compos Part B-Eng 177:107436
Liu XS, Sajda P, Saha PK, Wehrli FW, Bevill G, Keaveny TM, Guo XE (2008) Complete volumetric decomposition of individual trabecular plates and rods and its morphological correlations with anisotropic elastic moduli in human trabecular bone. J Bone Miner Res 23:223–235. https://doi.org/10.1359/Jbmr.071009
McCreadie BR, Morris MD, Chen TC, Rao DS, Finney WF, Widjaja E, Goldstein SA (2006) Bone tissue compositional differences in women with and without osteoporotic fracture. Bone 39:1190–1195. https://doi.org/10.1016/j.bone.2006.06.008
McNamara LM (2010) Perspective on post-menopausal osteoporosis: establishing an interdisciplinary understanding of the sequence of events from the molecular level to whole bone fractures. J R Soc Interface 7:353–372. https://doi.org/10.1098/rsif.2009.0282
Morgan EF, Bayraktar HH, Keaveny TM (2003) Trabecular bone modulus-density relationships depend on anatomic site. J Biomech 36:897–904. https://doi.org/10.1016/S0021-9290(03)00071-X
Niebur GL, Feldstein MJ, Yuen JC, Chen TJ, Keaveny TM (2000) High-resolution finite element models with tissue strength asymmetry accurately predict failure of trabecular bone. J Biomech 33:1575–1583
Nyman JS, Vashishth D (2018) Assessment of bone mass, structure, and quality in rodents. In: Bilezkian JP (ed) Primer on the metabolic bone diseases and disorders of mineral metabolism. Wiley, New York, pp 93–100
O'Connor DT et al (2016) Modeling orthotropic elasticity, localized plasticity and fracture in trabecular bone. Comput Mech 58:423–439. https://doi.org/10.1007/s00466-016-1301-3
Rachner TD, Khosla S, Hofbauer LC (2011) Osteoporosis: now and the future. Lancet 377:1276–1287. https://doi.org/10.1016/S0140-6736(10)62349-5
Riggs BL, Melton LJ (1995) The worldwide problem of osteoporosis–insights afforded by epidemiology. Bone 17:S505–S511. https://doi.org/10.1016/8756-3282(95)00258-4
Rizzoli R, Laroche M, Krieg MA, Frieling I, Thomas T, Delmas P, Felsenberg D (2010) Strontium ranelate and alendronate have differing effects on distal tibia bone microstructure in women with osteoporosis. Rheumatol Int 30:1341–1348. https://doi.org/10.1007/s00296-010-1542-y
Sabet FA, Najafi AR, Hamed E, Jasiuk I (2016) Modelling of bone fracture and strength at different length scales: a review. Interface Focus. https://doi.org/10.1098/rsfs.2015.0055
Sandino C, McErlain DD, Schipilow J, Boyd SK (2017) Mechanical stimuli of trabecular bone in osteoporosis: a numerical simulation by finite element analysis of microarchitecture. J Mech Behav Biomed 66:19–27. https://doi.org/10.1016/j.jmbbm.2016.10.005
Schwiedrzik JJ, Zysset PK (2013) An anisotropic elastic-viscoplastic damage model for bone tissue. Biomech Model Mechan 12:201–213. https://doi.org/10.1007/s10237-012-0392-9
Seeman E, Delmas PD (2006) Mechanisms of disease–bone quality–the material and structural basis of bone strength and fragility. New Engl J Med 354:2250–2261
Silva MJ, Brodt MD, Lynch MA, McKenzie JA, Tanouye KM, Nyman JS, Wang XD (2009) Type 1 diabetes in young rats leads to progressive trabecular bone loss, cessation of cortical bone growth, and diminished whole bone strength and fatigue life. J Bone Miner Res 24:1618–1627. https://doi.org/10.1359/Jbmr.090316
Stipsitz M, Zysset PK, Pahr DH (2020) Efficient materially nonlinear mu FE solver for simulations of trabecular bone failure. Biomech Model Mechan 19:861–874. https://doi.org/10.1007/s10237-019-01254-x
Tertuliano OA, Greer JR (2016) The nanocomposite nature of bone drives its strength and damage resistance. Nat Mater 15:1195–1202
Tertuliano OA, Edwards BW, Meza LR, Deshpande VS, Greer JR (2021) Nanofibril-mediated fracture resistance of bone Bioinspir Biomim 16:035001. https://doi.org/10.1088/1748-3190/abdd9d
Thurner PJ et al (2007) High-speed photography of compressed human trabecular bone correlates whitening to microscopic damage. Eng Fract Mech 74:1928–1941
Turner CH, Cowin SC, Rho JY, Ashman RB, Rice JC (1990) The fabric dependence of the orthotropic elastic-constants of cancellous bone. J Biomech 23:549–561. https://doi.org/10.1016/0021-9290(90)90048-8
Van Rietbergen B, Odgaard A, Kabel J, Huiskes R (1998) Relationships between bone morphology and bone elastic properties can be accurately quantified using high-resolution computer reconstructions. J Orthop Res 16:23–28. https://doi.org/10.1002/jor.1100160105
Verhulp E, Van Rietbergen B, Muller R, Huiskes R (2008) Micro-finite element simulation of trabecular-bone post-yield behaviour–effects of material model, element size and type. Comput Method Biomec 11:389–395. https://doi.org/10.1080/10255840701848756
Wang H et al (2013) Accuracy of individual trabecula segmentation based plate and rod finite element models in idealized trabecular bone microstructure. J Biomech Eng-T Asme 135:044502. https://doi.org/10.1115/1.4023983
Wang J et al (2015) Trabecular plates and rods determine elastic modulus and yield strength of human trabecular bone. Bone 72:71–80. https://doi.org/10.1016/j.bone.2014.11.006
Wang ZW et al (2017) Unique local bone tissue characteristics in iliac crest bone biopsy from adolescent idiopathic scoliosis with severe spinal deformity. Sci Rep-Uk 7:40265. https://doi.org/10.1038/srep40265
Werner B, Ovesy M, Zysset P (2019) An explicit microFE approach to investigate the post-yield behaviour of trabecular bone under large deformations. Int J Numer Meth Bio 35:e3188
Zysset P, Goulet R, Hollister S (1998a) A global relationship between trabecular bone morphology and homogenized elastic properties. J Biomech Eng 120:640–646
Zysset PK, Guo XE, Hoffler CE, Moore KE, Goldstein SA (1998b) Mechanical properties of human trabecular bone lamellae quantified by nanoindentation. Technol Health Care 6:429–432

Publisher's Note Springer Nature remains neutral with regard to jurisdictional claims in published maps and institutional affiliations.